

Inkjet-Printed Flexible Semitransparent Solar Cells with Perovskite and Polymeric Pillars

Naresh Kumar Pendyala, Shlomo Magdassi,* and Lioz Etgar*

Semitransparent perovskite solar cells are important for building-integrated photovoltaics. Most research is focused on glass substrates, which can be utilized as glass windows during the construction of the buildings. Herein, the fabrication of flexible and semitransparent perovskite-based solar cells is presented, which can be used for existing windows as retrofitting process. The transparency of the cells is obtained through printing transparent and noncolored “optical holes” at micrometric dimensions. The fabrication approach is based on inkjet printing pillars composed of polymerized *N*-vinylcaprolactam, followed by inkjet printing of a perovskite layer, to attain a digitally tuned semitransparency, all performed in open air. The printing compositions are tailored, including the solvents with a controlled volatility, and adding a surfactant to fit both the inkjet printing process and the vacuum-assisted perovskite crystallization. The flexible semitransparent solar cells achieve a power conversion efficiency (PCE) of 9.14%, with an average transmittance of 29.3%. Beyond transparency, the pillars also contributed to the mechanical properties: bending measurements reveal that the device without the pillars retains 71.4% of the PCE after 300 cycles compared to the pillared device which retains 90% of its initial PCE after 500 bendings.

1. Introduction


Perovskite solar cells (PSCs) with high power conversion efficiencies (PCEs, $\geq 25\%$) are attractive due to their solution processability, tunable optical properties, and viable cost when compared with silicon-based solar panels. In recent years, the field of semitransparent solar cells is emerging to provide building-integrated photovoltaic (BIPV) devices. So far most research is focused on glass substrates, thus the solar cell can be placed instead of the conventional glass windows, during the construction of the buildings. Here, we present the fabrication of flexible and semitransparent perovskite-based solar cells, which can be used for existing windows, via a retrofitting process. Beyond BIPV, such lightweight and flexible solar cells can be used in other applications, such as self-energy convertible tents, bags, and smart electronic gadgets. So far there are a few reports on semitransparent

rigid PSCs with moderate PCEs, in which the thickness of the perovskite layer and the chemical composition control the transparency of the solar cell.^[1–6] Solar cells with new structural designs, without changing chemical composition and layer thickness, could also deliver semitransparency; however, there could be a trade-off between transparency and the device’s PCE. Up to now, several solar cell designs based on dewetting, mesh-assisted, and nanopillar perovskite were reported, but only for glass-based solar cells. Snaith et al. have developed the dewetting approach; however, in this case, the PCEs (5–6%) were low and control over transparency is not possible.^[7,8] Yan et al. have developed the SiO₂ honeycomb scaffold template approach by combining self-assembly at the air–water interface and plasma etching. The porous SiO₂ template was prepared by etching the polystyrene while filling the pores with perovskite. The PCE of cells by this technique was $\approx 10\%$, and the average visible transmittance (AVT) of the active layer is 38%.^[9]

Moon et al. have developed nanopillar perovskite structures for semitransparent PSC fabrication. A template of anodized aluminum oxide was utilized, which provided the device’s semitransparency and improved the device’s stability. With this nanopillar-based structure, the semitransparent solar cell module reached $\approx 9\%$ PCE at AVT of 30% with a transparent ITO top contacts.^[10]

In our previous report, we used mesh-assisted perovskite grid-structured fabricating rigid semitransparent PSCs, in which the transparency of the perovskite film was controlled by varying the mesh size and the perovskite precursor concentration. This is a scalable approach, and the device was fabricated in ambient conditions, resulting in PCE of $\approx 10\%$, with a 28% AVT for the device without top metal contact.^[11,12] However, the void spaces of the perovskite grid were found to be responsible for shunt paths inside the solar cell. Therefore, for our recently modified solar cell design, we fabricated transparent polymeric pillars inside the perovskite layer by inkjet printing (IJP) of a polymerizable composition. The semitransparency of the rigid PSCs could be digitally controlled by varying the pillar area fraction. By this approach, after printing the pillars, the rest of the device fabrication, including the perovskite deposition, took place inside a glove box, resulting in cells having 11% efficiency with 24% AVT.^[13] The incorporation of polymers into the perovskite layer in the solar cell is also discussed in previous reports.^[14–17]

N. K. Pendyala, S. Magdassi, L. Etgar
Institute of Chemistry
Casali Center for Applied Chemistry
The Hebrew University of Jerusalem
Jerusalem 91904, Israel
E-mail: magdassi@mail.huji.ac.il; lioz.etgar@mail.huji.ac.il

 The ORCID identification number(s) for the author(s) of this article can be found under <https://doi.org/10.1002/solr.202200988>.

DOI: 10.1002/solr.202200988

In this work, we developed and studied flexible semitransparent solar cells. Recent reports on flexible perovskite reached high PCEs ($\approx 20\%$), but these cells were opaque.^[18–24] Here, we use flexible ITO substrate with a NiO_x hole transport layer (HTL), instead of the rigid glass ITOs, while the perovskite layer is deposited using the IJP technology, all done in an open-air atmosphere. The IJP method is well known for printing multimaterials in large industrial scale, only at the required amount of material, making the manufacturing cost viable with negligible materials wastage. Compared with the previous reports, with the current device configuration, a high FF of 73.55% was obtained. To the best of our knowledge, this is the first report of fabrication of flexible and semitransparent perovskite solar cells by IJP in air for utilization in BIPVs while enabling a retrofitting construction approach.

2. Results and Discussion

Figure 1 presents schematically the main fabrication steps for obtaining a flexible semitransparent perovskite solar cell. NiO_x nanoparticles (NPs) are deposited on a flexible PEN–ITO film substrate by spin coating. The *N*-vinylcaprolactam (NVC) monomer is printed by the inkjet printer, and then the NVC-ink is polymerized by UV light at room temperature to form transparent polymeric pillars, which serve as micrometric “optical holes.” In the next step, the perovskite solution (0.9 M, concentration determined via preliminary testing) using the same inkjet printer at ambient conditions is printed. The printing parameters of both NVC monomer and the perovskite solution are provided in (see Figure S3 and S4, Supporting Information, respectively). Immediately after printing the perovskite, a vacuum is applied using homemade vacuum unit (the vacuum unit can be seen

in Figure S5, Supporting Information). When vacuum is applied, the solvents in the perovskite layer start to evaporate within 5–15 s, and then crystallization occurs and completed after heating the substrate at 110 °C for 15 min. All these processes take place in open-air conditions. The solar cell is completed after spin coating the electron transport layer (ETL), i.e., phenyl-C61-butyric acid methyl ester (PCBM) and bathocuproine (BCP), followed by depositing a top metal contact (silver) using a thermal evaporator. The detailed experimental procedures are given in the Experimental Section.

The NiO_x NPs were synthesized following the report by Zhubing et al. (see the Experimental Section for the details).^[25] The NiO_x layer is deposited by spin coating the NiO_x dispersion onto the PEN/ITO substrate as shown in Figure 2b, while the inset image shows the NiO_x NPs taken by transmission electron microscope (TEM). The size of the NiO_x NPs is found to be in the range of 5–10 nm. Scanning electron microscope (SEM) images show the blank PEN/ITO (Figure 2a). The surface of the perovskite on top of the polymer pillars appears to be thin and non-uniform layer having small grain sizes. However, the perovskite layer which was deposited on top of NiO_x has closely packed large crystals and it seems more uniform (see Figure S14, Supporting Information). The difference in the grain size can be attributed to the amorphous nature of the polymer compared to the crystalline NiO_x . Figure 2c shows the top-view SEM of the perovskite layer which contains pinholes and large-size perovskite flakes.

In order to prevent these pinholes, we added the surfactant Triton X-114 at very low concentration (0.03 wt%) to the perovskite solution. The effect of surfactant concentration was evaluated (Figure S15, Supporting Information), and it was found that 0.03% yielded the best performance. This is the first time that Triton X-114 is used as surfactant in perovskite. The main role of the surfactant is to reduce the surface tension and to prevent

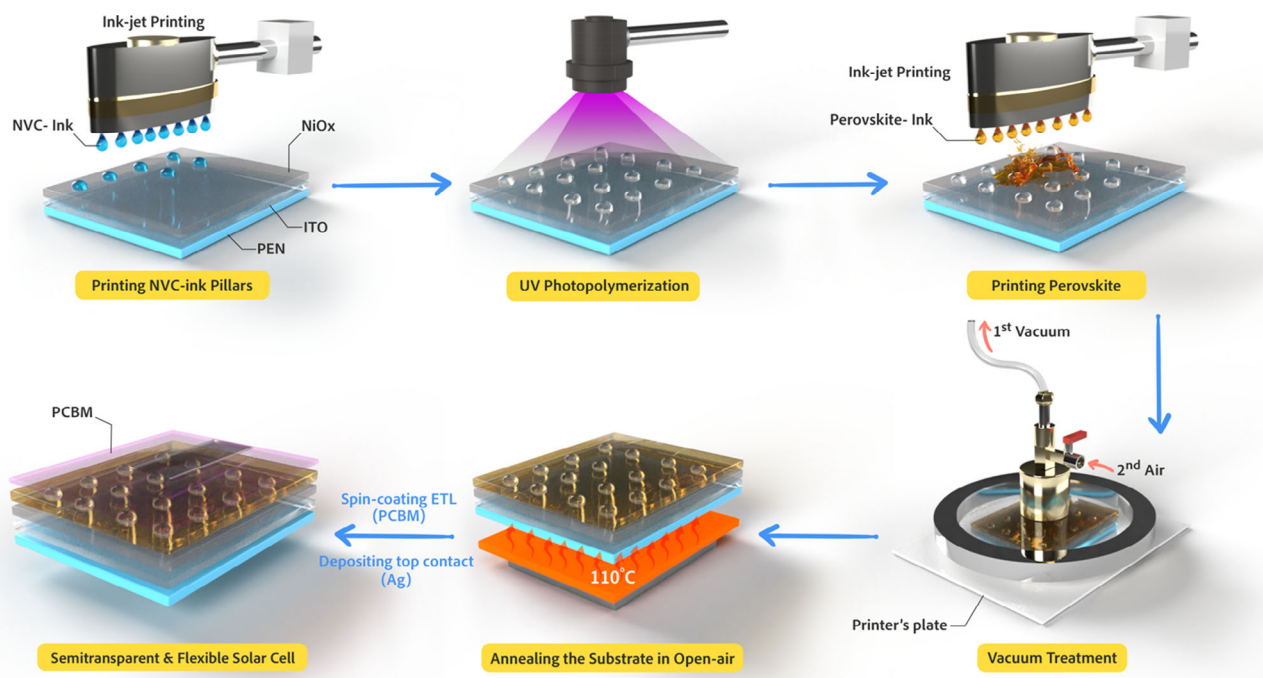


Figure 1. Schematic presentation of the main steps involved in the fabrication of the flexible semitransparent perovskite solar cell.

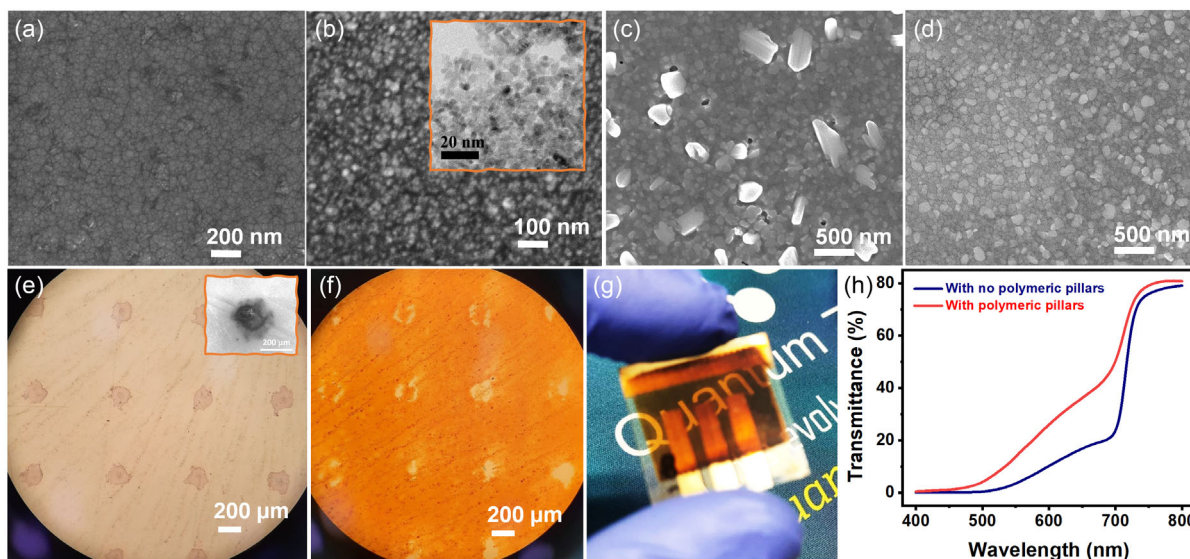


Figure 2. a) SEM surface images of PEN/ITO; b) NiO_x layer on top of ITO/PEN; c) the printed perovskite layer without surfactant; d) the printed perovskite layer with surfactant; e) microscopic images of the polymer pillars over NiO_x /ITO/PEN substrate (inset shows a single pillar SEM image); f) pillars with perovskite layer; g) a photograph of the flexible semitransparent perovskite solar cells; h) the transmittance curves for devices without the top metal contact.

unwanted pinholes that results from surface tension gradient which occur during solvent evaporation. Figure 2d presents the perovskite grains (with the addition of surfactant) which are uniform in size and without the pinholes in the layer. The function of surfactants on the perovskite crystallization process and the formation of grains with uniform sizes were reported in various studies.^[26–30] The optical microscope image shows the polymeric pillar patterns on PEN-ITO/ NiO_x (Figure 2e), where a single pillar with a diameter of about 200 μm can be seen at the inset of Figure 2e. The pillars embedded within the perovskite layer can be seen in Figure 2f. In our previous report, pillars with size of 500–600 μm have influenced the AVT as well as the PCE of the device, where the perovskite precursors were dissolved in DMF and DMSO. Moreover, in our previous work, the perovskite was deposited by spin coating approach compared to IJP in the current work.^[13]

A photograph of the flexible semitransparent perovskite solar cell is shown in Figure 2g. The transmittance of the perovskite cell with and without pillars was compared between 400 and 800 nm wavelength (entire visible spectral region, Figure 2h). It was found that the device without the pillars has an AVT of 21%, whereas the device with pillars shows an AVT of 32%. For the same devices, the calculated average photopic transmittance (APT) is found to be 23.6% and 32.6% for devices without and with pillars, respectively. The increased transmittance of the pillared device is attributed to the transparent voids, which allow free passage of light.

Beyond issues related to the printability of the perovskite solution, the solvent composition is crucial in the perovskite crystallization and thus influences the solar cell efficiency. Most of the articles report on DMF and DMSO as cosolvents which are recognized as the best solvents combination for organic–inorganic hybrid perovskite solar cells.^[31–35] However, few articles reported high PCEs using other solvent combinations. Sang et al. reported

on the use of perovskite solution composed of DMSO together with γ -butyrolactone, in which the DMSO assisted in the formation of the MAI– PbI_2 –DMSO intermediate phase, which could be transferred to crystallized perovskite after the addition of toluene.^[36] In another report by Jihuai et al., along with DMF and DMSO, a third solvent, i.e., *N*-methyl-2-pyrrolidone (NMP), was introduced into the solvent mixture which improved the device's performance.^[37]

DMSO has high-boiling point and is not suitable for the large-scale printing industry. Therefore, in an attempt to replace the DMSO, we have evaluated three protic solvents which are commonly used in industrial printing, including IJP: 1-methoxy-2-propanol (PM), 2-ethoxyethanol (EE), and methoxy propyl acetate (PMA). These solvents have been chosen after preliminary testing of various common solvents used in industrial printing formulations, based on their good wettability during IJP. The perovskite precursor solution was prepared using DMF alone as well as DMF in combination with the three solvents. The absorbance measured for the perovskite films is shown in Figure 3a. The absorbance onset was found to be slightly red-shifted for EE compared to the other solvents. However, the perovskite conversion was found to be the best in the case of the solvents mixture which contain DMF with PM (boiling point 120 °C). The coordination between PM and lead halide ($\text{Pb}(\text{IBr})_2$) was elucidated from the Fourier-transform infrared spectroscopy (FTIR) as presented in Figure S6, Supporting Information. The reduced intensity of hydrogen bonding corresponds to the peak position at 3400 cm^{-1} for PM- $\text{Pb}(\text{IBr})_2$ compared with PM alone. As a result, it can be concluded on increased interactions between PM and Pb. Moreover, the shift of the stretching frequency at 1102 to 1090 cm^{-1} corresponds to the alkoxy group which supports the alkoxy coordination to the lead halide (inset Figure S6, Supporting Information). The top-view SEM images of the perovskite films crystallize from DMF alone,

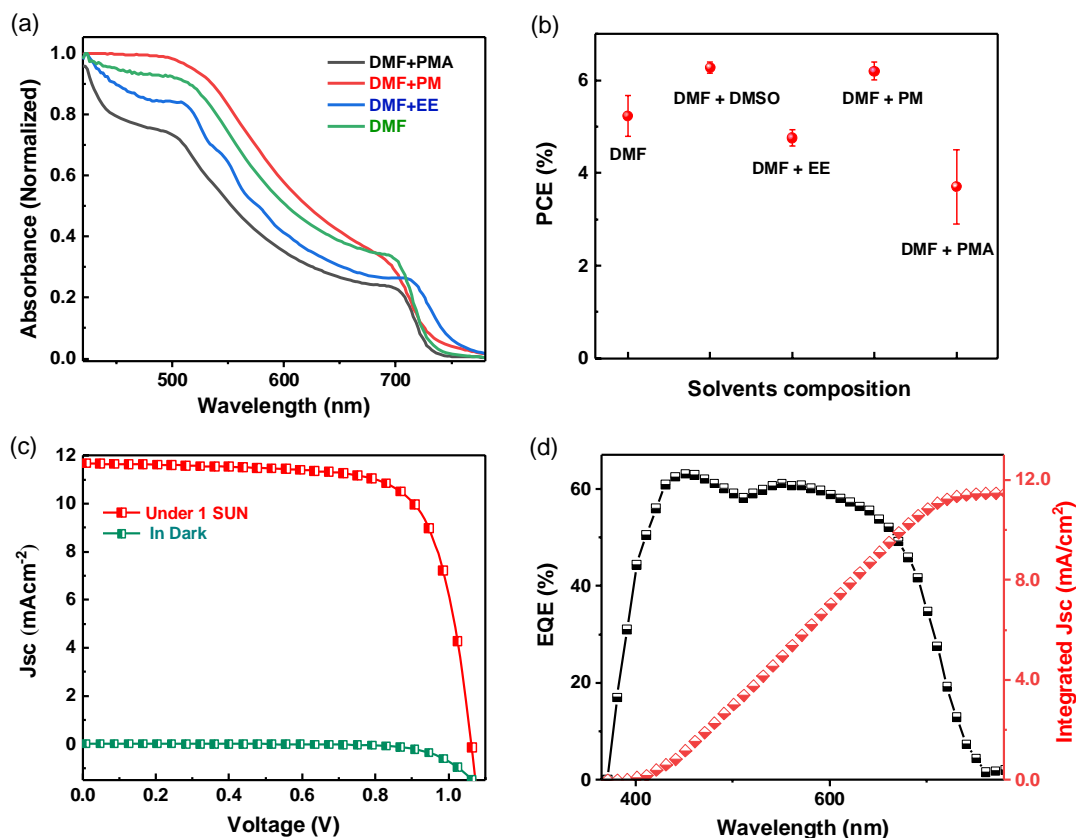


Figure 3. a) The absorbance of the perovskite films crystallize from solution with DMF and a combination of other solvents as described in the main text. b) The PCE of the perovskite printed on flexible semitransparent solar cells when the DMSO was replaced with the studied solvents. c) J - V curve in the dark and under 1 sun illumination of the champion flexible semitransparent perovskite solar cell. d) EQE and the integrated J_{sc} were obtained for the flexible semitransparent perovskite solar cell.

DMF + PM, DMF + PMA, and DMF + EE can be observed in Figure S7, Supporting Information. The best morphology of perovskite crystals with uniform grains, without pinholes, can be found for the DMF + PM, compared with the other perovskite's solvents combination. To the best of our knowledge, this is the first time PM is used as a solvent for perovskite replacing the DMSO. It was found that combining PM with DMF (4:1; i.e., 20% PM) led to the improvement of the PCE (Figure 3b) when compared with DMF alone and DMF together with other protic solvents such as EE and PMA. The PM replaced the DMSO and eased the perovskite nucleation under low vacuum conditions making the perovskite ink formulation, suitable for IJP. After printing the perovskite solution, the crystallization was simply initiated under a vacuum instead of the antisolvent technique. The PM favored quick evaporation and thus improved the perovskite crystallization which occurs within a short time of 15 s. In addition, as discussed earlier, the surfactant Triton X-114 was added to the perovskite solution and improved its morphology which supports the improved PCE from 6.39% to 9.14% with this surfactant. The Triton X-114 was the best surfactant among several other surfactants that were evaluated, FC-4430, BYK-333, Triton x-100, S-75, and Tween-20. The PCE of these solar cells with the different surfactants can be observed in Figure S9, Supporting Information.

The J - V curves measured for the champion cell under dark and under 1 sun illumination, having an AVT of 29.3%, are shown in Figure 3c. The short-circuit current density (J_{sc}), open-circuit voltage (V_{oc}), fill factor (FF), and the PCE values calculated to be 11.72 mA cm⁻², 1.06 V, 73.55%, and 9.14%, respectively (Table 1). The external quantum efficiency (EQE) is shown in Figure 3d with an integrated J_{sc} of 11.5 mA cm⁻², supporting the J_{sc} value obtained from J - V measurement. The hysteresis curve of this cell is negligible and can be observed in Figure S13, Supporting Information.

To realize the statistics of the solar cell performance, several NVC pillar-based flexible semitransparent solar cells were fabricated by IJP. The PV parameters such as PCE (Figure 4a), J_{sc} (Figure 4b), V_{oc} (Figure 4c), and FF (Figure 4d) are presented compiled for the ten devices with AVT greater than 28%.

Table 1. The PV parameters and the AVT of the flexible semitransparent solar cell with and without the polymer pillars.

| Cell structure | V_{oc} [V] | J_{sc} [mA cm ⁻²] | FF [%] | Eff [%] | AVT [%] |
|-----------------|--------------|---------------------------------|--------|---------|---------|
| without pillars | 1.02 | 11.72 | 66.97 | 8.03 | 21 |
| With pillars | 1.06 | 11.7 | 73.55 | 9.14 | 29.3 |

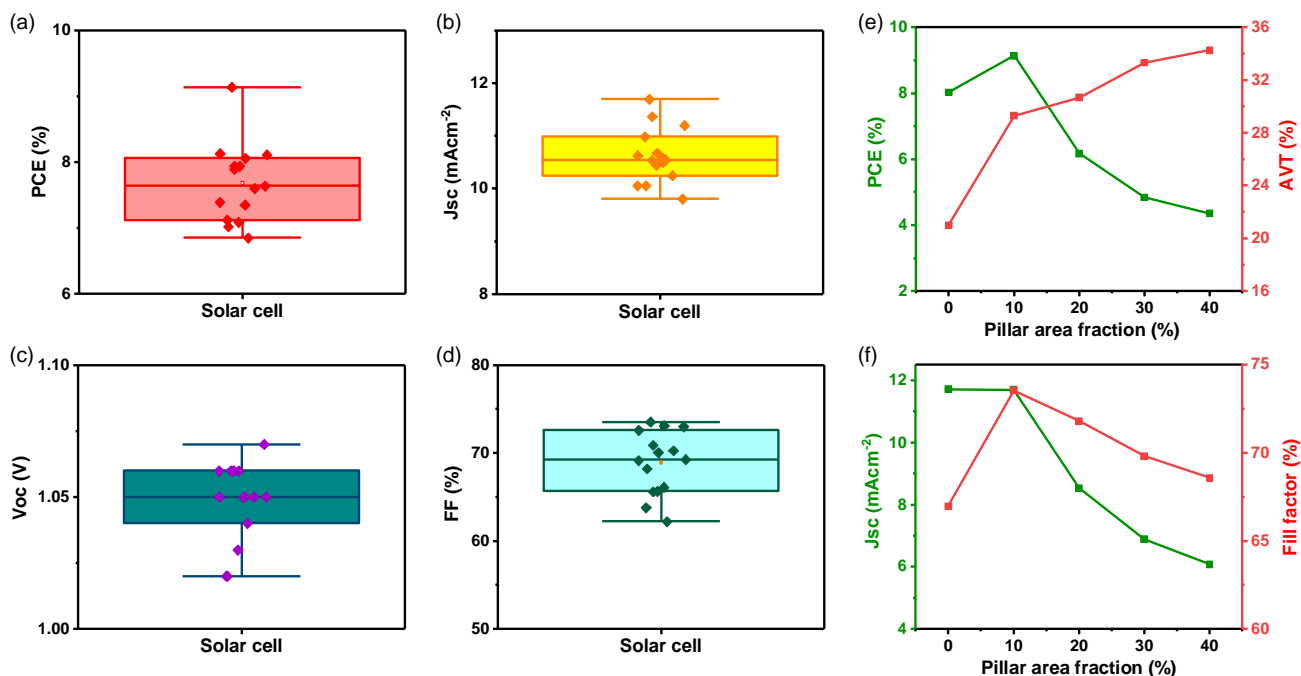


Figure 4. Statistical data for 15 flexible semitransparent solar cells: a) PCE; b) short-circuit current density; c) open-circuit voltage; d) FF; e) PCE and AVT versus NVC pillar area; f) J_{sc} and FF versus NVC pillar area fraction.

Even though the champion PCE is 9%, most of the PCE values for the flexible semitransparent cells range between 7% and 8%, while the average value is 7.69% with an average AVT of 30%. The J_{sc} values range between 9 and 12 mAcm^{-2} , and the average J_{sc} value is 10.62 mAcm^{-2} . The low J_{sc} values are attributed to the voids occupied by the transparent pillars. The V_{oc} is observed to be more than 1 V for all ten devices, with an average value of 1.048 V. These pillared devices have relatively high V_{oc} , even though they incorporated pillars in the perovskite layer. The quality of the interfaces can be understood from the FF values. Here, the FF values are found to be more than 60% for all the devices, with an average value of 68.9%. When comparing the best devices with and without the polymeric pillars, the FF values are found to be higher in the case of pillar-based devices. This represents the improved interfacial quality for the pillared perovskite layer. Overall, we have successfully fabricated a pillar-embedded flexible semitransparent solar cells, with an average AVT of 30% and an average PCE of 7.69%, while the wet fabrication steps are made in the open air. The tunability of the device by changing the pillar area was further studied by varying the pillar area on top of NiO_x layer. As the pillar area fraction increased from 0 to 40%, the AVT of the device increased gradually from 21% to 34.2%, while the PCE increased at 10% pillars' area fraction; however, then, it gradually decreased to 4.35% (see Figure 4e). This can be explained by the slight increase of the FF for the cells with a 10% pillars' area fraction, as discussed before the pillars contribute to the film formation which increase the FF. For all the cases, the V_{oc} was almost constant between 1.01 and 1.06 V. The FF of the devices was always found to be higher for devices with pillars than devices without them. Therefore, we can conclude that the reduced PCE can be attributed to the decrease in the J_{sc}

values when increasing the pillar area (see Figure 4f). We have also calculated the light utilization efficiency (LUE; the product of PCE and AVT of a solar cell) and plotted PCE and LUE as a function of pillar area fraction (see Figure S10, Supporting Information). The best LUE for the flexible PSC is 2.67% (obtained for the cell with the best PCE of 9.13%). The LUE calculated for flexible solar cell without the polymeric pillars is 1.68%. Thus, a 58% enhancement in LUE is observed for the best cell with 10% pillar area fraction when compared to the cell without polymeric pillars. Based on the AVT and the PCE values reported in the literature for perovskite solar cells, we have calculated the LUE of these cells and compared them with the LUE of our flexible transparent solar cell. The LUE of our cell is 2.67%, whereas the average value of LUE for the other reported perovskite solar cells is 2.04%. The graph which summarizes the LUE observed in the literature can be found in Figure S11, Supporting Information.

The operational stability of the fabricated flexible semitransparent solar cells was realized from the PCE measurements upon bending cycles. The solar cell was bent by a supporting rod (radius of 8 mm). **Figure 5a** shows the PV parameters (normalized V_{oc} , J_{sc} , FF, and PCE) versus the number of bending cycles. The PCE was found to be retained 90.97% after 500 bending cycles. The efficiency of the device seems to be stable during the bending test. The V_{oc} was slightly decreased to 97.5% compared to its initial value, and the J_{sc} and FF values were reduced to 95.7% and 97.66%, respectively, when compared to their initial values. For comparison, we have performed the bending test for devices without the pillars, which show a gradually decreasing PCE over bending. As can be seen in Figure S12, Supporting Information, the PCE was reduced to 71.4% after 300 bending

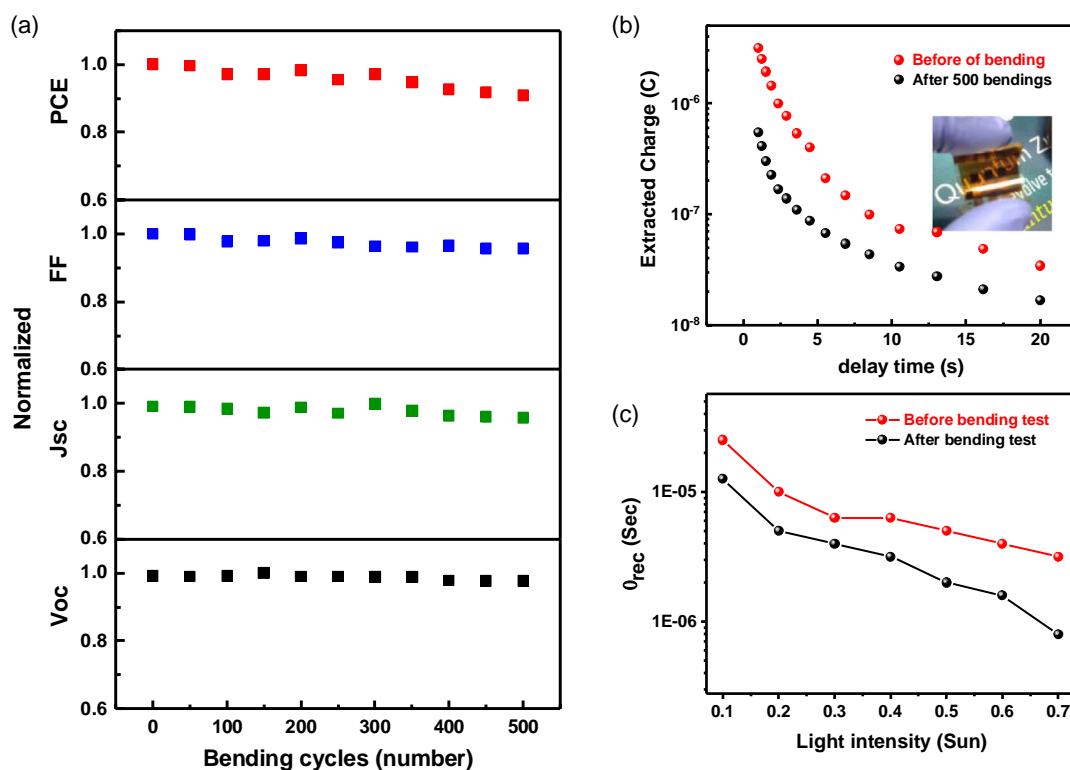


Figure 5. a) Normalized PV parameters as a function of the bending cycles; b) charge extraction before and after 500 bending cycles; inset shows an optical photograph of the flexible cell while in bending mode; c) electron recombination lifetime obtained for the flexible semitransparent solar cell with the best PCE.

cycles. Thus, we can suggest that the pillars assist in the mechanical flexibility of the perovskite film by forming a barrier for cracks in the film. However, for cells without pillars, some cracks are formed and continue to progress without the barrier formed by the NVC pillars. Therefore, it can be assumed that the bending stability is attributed to the presence of polymeric pillars in the cells.

To further elucidate the mechanism during the bending test, charge extraction and intensity-modulated photovoltage spectroscopy (IMVS) measurements were performed before and after 500 cycles of bending. The charge extraction measurement can be seen in Figure 5b, where there is a clear indication that the cells after 500 bending cycles have a higher rate of recombination compared to cells before bending. The IMVS measurement provides information on the charge recombination lifetime of the cells at different light intensities. Figure 5c shows a shorter recombination lifetime for the cells after 500 bending cycles compared to cells before the bending test. The higher recombination rate and shorter recombination lifetime after 500 bending cycles for the flexible semitransparent solar cells are attributed to the partial degradation of interfaces between the ETL and perovskite layer as well as perovskite layer and HTL, respectively. Still, the PV parameters show good stability as discussed above.

The stability of the devices was tested by measuring the PCE under continuous 1 sun illumination. Every 20 min of continuous illumination, the light was turned off for 5 min, and then the

PCE measured again under illumination (Figure 6a). While compared to its initial PCE, when the device is placed under illumination, the device remained with 88% efficiency after the first 20 min of illumination, and after 5 min in the dark the device recovered to its initial PCE. Following the second and the third cycles, the same effect of recovery was observed; however, the PCE did not return completely to its initial value. The J_{sc} and V_{oc} did not show any decrease during these light on and off cycles, while the FF shows the same trend as the PCE which can suggest that the interfaces inside the device can be the reason for that slight degradation upon the illumination cycles.

In addition, we also studied the stability of the devices, without any encapsulation, while stored inside and outside N_2 -filled glove box. The devices stored inside the glove box retained 93% of PCE, whereas devices stored outside, i.e., in an open-air atmosphere (humidity ≈ 40 –50%), retained 73% after 240 h (Figure 6b). The corresponding V_{oc} of the devices retained 99% and 80% after 240 h (Figure 6c), where the J_{sc} of the devices retained 99% and 94% after 240 h (Figure 6d) stored inside and outside the glove box, respectively. The FF values are found to be the same in both cases, retained 81% (Figure 6e). In general, the unencapsulated devices stored in the glove box showing excellent stability while the unencapsulated devices stored outside show decent stability where the main reduction was observed in the FF. As discussed also in the case of the bending stability test, the FF is more affected by the environment parameters due to the pillar structure.

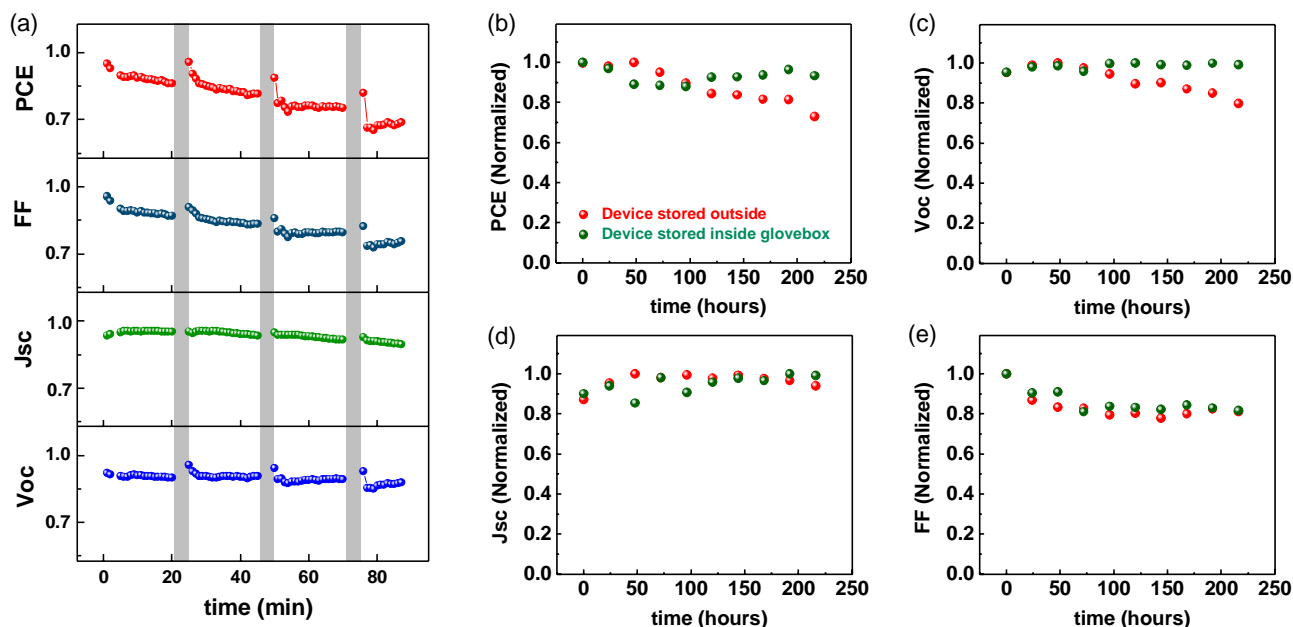


Figure 6. a) PCE of the device under continuous 1 sun illumination for 20 min and then kept in the dark for 5 min. The PV parameters were collected every minute. Unencapsulated devices stored in the glove box (green) and outside (red) were measured every week and 24 hr, respectively. b) PCE, c) V_{oc} , d) J_{sc} , and e) FF.

3. Conclusions

The unique structure of semitransparent flexible perovskite solar cells was fabricated, where polymeric pillars and the perovskite solutions are printed by the inkjet printer. All the solar cell steps were made by wet fabrication and performed in air. The DMSO solvent with a high boiling point was replaced with a volatile solvent, PM, that is widely used in the industry, to ease the crystallization of the perovskite layer during simple vacuum treatment. The flexible semitransparent perovskite solar cell has shown a PCE of 9.14% with an AVT of 29.3%. Overall, this work involves solvent engineering and upgraded the conceptual design of semitransparent perovskite solar cell fabrication in an open-air atmosphere on flexible substrates using IJP technology. Besides enhancing the AVT of the device, the pillars also attributed to the device's stability during bending cycles. Thus, this work brings a new value to the emerging field of BIPVs while enabling retrofitting of existing building windows.

4. Experimental Section

Materials: All chemicals were commercially available, procured, and used for the experiments without further purifications: nickel (II) nitrate hexahydrate ($\text{Ni}(\text{NO}_3)_2 \cdot 6\text{H}_2\text{O}$: 97%, Sigma-Aldrich), NVC (98%, Sigma-Aldrich), diphenyl(2,4,6-trimethylbenzoyl)phosphine oxide (TPO: BASF, Germany), triphenylphosphine (99%, Strem Chemicals), zinc dust (<10 μm , >98%, Sigma-Aldrich), cesium iodide (CsI: 99.999%, Sigma-Aldrich), formamidinium iodide (FAI: 99.99%, Sigma-Aldrich), lead(II) iodide (PbI_2 : 99%, Sigma-Aldrich), lead(II) bromide (PbBr_2 : >98%, Sigma-Aldrich), phenyl-C61-butyrac acid methyl ester (PCBM: 99.5%, Ossila), bathocuproine (BCP: Sublimed), hydrochloric acid (37%, Sigma-Aldrich), and anhydrous solvents like *N,N*-dimethylformamide (DMF: 99.8%, Acros Organics), 1-methoxy-2-propanol' (PM, 99.5%,

Sigma-Aldrich), 2-ethoxyethanol (EE; 99%, Sigma-Aldrich), and methoxy propyl acetate (PMA, 99.5%, Aldrich), dimethyl sulfoxide (DMSO: 99.7+%, Acros Organics), anisole (99.7%, Sigma-Aldrich), ethanol (99%, Fisher Scientific, UK), and isopropanol (>99.7%, Daejung Chemicals-Korea). The conducting PEN/ITO substrates (15 Ohm/sq) were procured from Peccell (Japan).

NiO_x Synthesis: Nickel oxide (NiO_x) was synthesized by following a previous report.^[25] In brief, $\text{Ni}(\text{NO}_3)_2 \cdot 6\text{H}_2\text{O}$ (3 g) dissolved in 120 mL of deionized water (DI- H_2O) and stirred to get a clear green solution. The pH of this solution was adjusted to 10 by the addition of 1M NaOH and the obtained green precipitate was washed 3 times with DI H_2O to remove the reactants and then dried in a vacuum oven at 70 °C (overnight). The obtained green pellets were calcinated at 275 °C for 2 hrs, and finally received the dark gray pellets and labeled as NiO_x ; after grinding, dispersed into 10% IPA/DI H_2O and used as hole transport material for solar cell fabrication.

NVC-Ink Formulation: As we have reported in our previous report,^[13] NVC monomer (4 g), photoinitiator (4 wt% TPO, 0.16 g), and surface curing agent (9.2 wt% triphenylphosphine, 0.368 g) were taken into a glass vial. After shaking it well for 10 min, the solid mixture was turned into a homogeneous liquid ink. The freshly prepared ink became viscous after 10 min, diluted further using anisole (1:2 v/v), and ink used to fill the printer cartridge.

Perovskite Precursor Solution: 0.9 M Perovskite ($\text{Cs}_{0.2}\text{FA}_{0.8}(\text{PbI}_{0.6}\text{Br}_{0.4})_3$) solution was prepared by the addition of CsI (46.73 mg), FAI (123.84 mg), PbI_2 (249.48 mg), and PbBr_2 (132.14 mg) into a vial with 0.9 mL DMF, and 0.1 mL PM. The perovskite solution was stirred for 4 hrs at 70 °C, and to this solution, after cooling to room temperature, Triton X-114 surfactant (0.03 wt% using a prediluted (1 wt%) surfactant solution of DMF) was added. This solution, after the addition of surfactant, was stirred (800 rotations per min., at 70 °C) for 5 min. and filtered (filter pore dia. 0.4 μm) before filling into the printer's cartridge.

Solar Cell Fabrication: Prior to the solar cell fabrication, the flexible PEN/ITO substrates with required dimensions were etched to obtain the required ITO patterns using Zn/HCl and then cleaned placing them into a soap solution, acetone, and ethanol (using an ultrasonic bath) 10 min each. After drying with a compressed air, these substrates were

treated with O₂ plasma (30%, 90 s). A 30 mg NiO_x powder was well dispersed in 10% IPA (1 mL) by placing it in the bath sonication for 6–8 hrs maintaining the bath temperature below 35 °C and deposited onto the plasma-treated PEN–ITO substrates without further delay, followed by heated placing them on to a hot plate (110 °C, 15 min). The NVC monomer ink was printed and polymerized by UV light (constant illumination for 60 s with a center wavelength of 395 nm with an intensity of 50 mW cm⁻²). Then the NVC-ink cartridge was replaced by the perovskite-ink cartridge and the printing file was updated in the software. The perovskite was printed at room temperature over the polymer-pillared PEN/ITO/NiO_x substrates after the plasma treatment. Without any further delay, the vacuum unit (shown in Figure 1) was placed over the substrate and a vacuum was applied for 10 s to nucleate the perovskite film. Then, the colored substrate was transferred onto a hot plate (110 °C, 10 min).

Supporting Information

Supporting Information is available from the Wiley Online Library or from the author.

Acknowledgements

The authors would like to thank the financial support of the Lady Davis fellowship for N.K.P. and the Israeli Ministry of Energy and Infrastructure are highly appreciated (grant no. 221-11-044).

Conflict of Interest

The authors declare no conflict of interest.

Data Availability Statement

The data that support the findings of this study are available in the supplementary material of this article.

Pictures related to PEN–ITO supported on the glass substrate, NiO_x NPs after calcination, and its solution, homemade vacuum unit, and the perovskite layer over PEN–ITO/NiO_x substrate before and after the plasma treatments; and the printing recipes were provided.

Keywords

flexible solar cells, inkjet printing, perovskite solar cells, semitransparency, solvent engineering

Received: November 1, 2022

Revised: December 27, 2022

Published online:

- [1] C. Roldan-Carmona, O. Malinkiewicz, R. Betancur, G. Longo, C. Momblona, F. Jaramillo, L. Camacho, H. J. Bolink, *Energy Environ. Sci.* **2014**, *7*, 2968.
- [2] L. Yuan, Z. Wang, R. Duan, P. Huang, K. Zhang, Q. Chen, N. K. Allam, Y. Zhou, B. Song, Y. Li, *J. Mater. Chem. A* **2018**, *6*, 19696.
- [3] M. T. Hörantner, W. Zhang, M. Saliba, K. Wojciechowski, H. J. Snaith, *Energy Environ. Sci.* **2015**, *8*, 2041.
- [4] A. A. Husain, W. Z. W. Hasan, S. Shafie, M. N. Hamidon, S. S. Pandey, *Renewable Sustainable Energy Rev.* **2018**, *94*, 779.
- [5] C. D. Bailie, M. G. Christoforo, J. P. Mailoa, A. R. Bowering, E. L. Unger, W. H. Nguyen, J. Burschka, N. Pellet, J. Z. Lee, M. Grätzel, R. Noufi, *Energy Environ. Sci.* **2015**, *8*, 956.
- [6] M. Nakamura, C. C. Lin, C. Nishiyama, K. Tada, T. Bessho, H. Segawa, *ACS Appl. Energy Mater.* **2022**, *5*, 8103.
- [7] G. E. Eperon, V. M. Burlakov, A. Gorieli, H. J. Snaith, *ACS Nano* **2014**, *8*, 591.
- [8] G. E. Eperon, D. Bryant, J. Troughton, S. D. Stranks, M. B. Johnston, T. Watson, D. A. Worsley, H. J. Snaith, *J. Phys. Chem. Lett.* **2015**, *6*, 129.
- [9] L. Zhang, M. T. Hörantner, W. Zhang, Q. Yan, H. J. Snaith, *Sol. Energy Mater. Sol. Cells* **2017**, *160*, 193.
- [10] H. C. Kwon, S. Ma, S. C. Yun, G. Jang, H. Yang, J. Moon, *J. Mater. Chem. A* **2020**, *8*, 1457.
- [11] S. Aharon, M. Layani, B. E. Cohen, E. Shukrun, S. Magdassi, L. Etgar, *Adv. Mater. Interfaces* **2015**, *2*, 1500118.
- [12] M. Rai, S. Rahmany, S. S. Lim, S. Magdassi, L. H. Wong, L. Etgar, *J. Mater. Chem. A* **2018**, *6*, 23787.
- [13] N. K. Pendyala, S. Magdassi, L. Etgar, *ACS Appl. Mater. Interfaces* **2021**, *13*, 30524.
- [14] F. Bisconti, A. Giuri, L. Dominici, S. Carallo, E. Quadri, P. Biagini, A. Listorti, C. E. Corcione, S. Colella, A. Rizzo, *Nano Energy* **2021**, *89*, 106406.
- [15] O. Almora, D. Baran, G. C. Bazan, C. Berger, C. I. Cabrera, K. R. Catchpole, S. Erten-Ela, F. Guo, J. Hauch, A. W. Ho-Baillie, T. J. Jacobsson, *Adv. Energy Mater.* **2021**, *11*, 2002774.
- [16] O. M. Alkudhari, A. Altujjar, M. Z. Mokhtar, B. F. Spencer, Q. Chen, A. G. Thomas, N. W. Hodson, X. Wang, P. Hill, J. Jacobs, R. J. Curry, *J. Mater. Chem. A* **2022**, *10*, 10227.
- [17] G. Giuliano, A. Bonasera, G. Arrabito, B. Pignataro, *Sol. RRL* **2021**, *5*, 2100702.
- [18] G. Tang, F. Yan, *Nano Today* **2021**, *39*, 101155.
- [19] Q. Dong, M. Chen, Y. Liu, F. T. Eickemeyer, W. Zhao, Z. Dai, Y. Yin, C. Jiang, J. Feng, S. Jin, S. F. Liu, *Joule* **2021**, *5*, 1587.
- [20] Y. Hu, T. Niu, Y. Liu, Y. Zhou, Y. Xia, C. Ran, Z. Wu, L. Song, P. Müller-Buschbaum, Y. Chen, W. Huang, *ACS Energy Lett.* **2021**, *6*, 2917.
- [21] X. Li, Z. Shi, F. Behrouznejad, M. Hatamvand, X. Zhang, Y. Wang, F. Liu, H. Wang, K. Liu, H. Dong, F. Mudasar, *J. Energy Chem.* **2022**, *67*, 1.
- [22] T. Xue, G. Chen, X. Hu, M. Su, Z. Huang, X. Meng, Z. Jin, J. Ma, Y. Zhang, Y. Song, *ACS Appl. Mater. Interfaces* **2021**, *13*, 19959.
- [23] S. Wu, Z. Li, J. Zhang, X. Wu, X. Deng, Y. Liu, J. Zhou, C. Zhi, X. Yu, W. C. Choy, Z. Zhu, *Adv. Mater.* **2021**, *33*, 2105339.
- [24] Z. Wang, Y. Lu, Z. Xu, J. Hu, Y. Chen, C. Zhang, Y. Wang, F. Guo, Y. Mai, *Adv. Sci.* **2021**, *8*, 2101856.
- [25] W. Chen, Y. Zhou, L. Wang, Y. Wu, B. Tu, B. Yu, F. Liu, H. W. Tam, G. Wang, A. B. Djurišić, L. Huang, *Adv. Mater.* **2018**, *30*, 1800515.
- [26] H. Ying, Y. Liu, Y. Dou, J. Zhang, Z. Wu, Q. Zhang, Y. B. Cheng, J. Zhong, *Front. Optoelectron.* **2020**, *13*, 272.
- [27] Q. Wang, H. Li, J. Zhuang, H. Guo, X. Liu, Z. Guo, X. Gong, H. Li, *J. Mater. Sci.* **2020**, *55*, 14761.
- [28] C. Y. Chang, Y. C. Chang, W. K. Huang, K. T. Lee, A. C. Cho, C. C. Hsu, *Chem. Mater.* **2015**, *27*, 7119.
- [29] K. Liu, Q. Liang, M. Qin, D. Shen, H. Yin, Z. Ren, Y. Zhang, H. Zhang, P. W. Fong, Z. Wu, J. Huang, *Joule* **2020**, *4*, 2404.
- [30] T. Wang, M. Xie, S. Abbasi, Z. Cheng, H. Liu, W. Shen, *J. Power Sources* **2020**, *448*, 227584.
- [31] A. J. Doolin, R. G. Charles, C. S. De Castro, R. G. Rodriguez, E. V. Péan, R. Patidar, T. Dunlop, C. Charbonneau, T. Watson, M. L. Davies, *Green Chem.* **2021**, *23*, 2471.
- [32] R. Liu, K. Xu, *Micro Nano Lett.* **2020**, *15*, 349.
- [33] Y. H. Seo, E. C. Kim, S. P. Cho, S. S. Kim, S. I. Na, *Appl. Mater. Today* **2017**, *9*, 598.

- [34] Y. Deng, C. H. Van Brackle, X. Dai, J. Zhao, B. Chen, J. Huang, *Sci. Adv.* **2019**, *5*, eaax7537.
- [35] J. Jiang, J. M. Vicent-Luna, S. Tao, *J. Energy Chem.* **2022**, *68*, 393.
- [36] N. J. Jeon, J. H. Noh, Y. C. Kim, W. S. Yang, S. Ryu, S. I. Seok, *Nat. Mater.* **2014**, *13*, 897.
- [37] T. Wu, J. Wu, Y. Tu, X. He, Z. Lan, M. Huang, J. Lin, *J. Power Sources* **2017**, *365*, 1.